Decreasing net primary production due to drought and slight decreases in solar radiation in China from 2000 to 2012

AGU PUBLICATIONS

JGR

Journal of Geophysical Research: Biogeosciences

RESEARCH ARTICLE
10.1002/2016JG003417

Key Points:
- The global MODIS NPP product can be improved by using local daily meteorology data sets and biome-specific parameters
- An overall decreasing NPP was largely dominated by forests over southern China which offset smaller increases in Northern China ecosystems
- Reductions in NPP were largely due to decreases in solar radiation (82%), rather than the commonly expected effects of drought (18%)

Supporting Information:
- Supporting Information S1

Correspondence to:
J. Wang,
jbwang@igsnrr.ac.cn

Citation:
Wang, J., J. Dong, Y. Yi, G. Lu, J. Oyler, W. K. Smith, M. Zhao, J. Liu, and S. Running (2017), Decreasing net primary production due to drought and slight decreases in solar radiation in China from 2000 to 2012, *J. Geophys. Res. Biogeosci.*, *122*, 261–278, doi:10.1002/2016JG003417.

Received 21 MAR 2016
Accepted 2 JAN 2017
Accepted article online 9 JAN 2017
Published online 30 JAN 2017

Decreasing net primary production due to drought and slight decreases in solar radiation in China from 2000 to 2012

J. Wang[1], J. Dong[2], Y. Yi[3], G. Lu[4], J. Oyler[3], W. K. Smith[5], M. Zhao[3], J. Liu[1], and S. Running[3]

[1]Key Laboratory of Ecosystem Network Observation and Modeling, Institute of Geographic Sciences and Natural Resources Research, Chinese Academy of Sciences, Beijing, China, [2]Key Laboratory of Land Surface Pattern and Simulation, Institute of Geographic Sciences and Natural Resources Research, Chinese Academy of Sciences, Beijing, China, [3]Numerical Terradynamic Simulation Group, College of Forestry and Conservation, University of Montana, Missoula, Montana, USA, [4]Department of Grassland Science, Agriculture and Animal Husbandry College, Qinghai University, Xining, China, [5]School of Natural Resources and the Environment, University of Arizona, Tucson, Arizona, USA

Abstract Terrestrial ecosystems have continued to provide the critical service of slowing the atmospheric CO_2 growth rate. Terrestrial net primary productivity (NPP) is thought to be a major contributing factor to this trend. Yet our ability to estimate NPP at the regional scale remains limited due to large uncertainties in the response of NPP to multiple interacting climate factors and uncertainties in the driver data sets needed to estimate NPP. In this study, we introduced an improved NPP algorithm that used local driver data sets and parameters in China. We found that bias decreased by 30% for gross primary production (GPP) and 17% for NPP compared with the widely used global GPP and NPP products, respectively. From 2000 to 2012, a pixel-level analysis of our improved NPP for the region of China showed an overall decreasing NPP trend of 4.65 Tg C a^{-1}. Reductions in NPP were largest for the southern forests of China (−5.38 Tg C a^{-1}), whereas minor increases in NPP were found for North China (0.65 Tg C a^{-1}). Surprisingly, reductions in NPP were largely due to decreases in solar radiation (82%), rather than the more commonly expected effects of drought (18%). This was because for southern China, the interannual variability of NPP was more sensitive to solar radiation (R^2 in 0.29–0.59) relative to precipitation ($R^2 < 0.13$). These findings update our previous knowledge of carbon uptake responses to climate change in terrestrial ecosystems of China and highlight the importance of shortwave radiation in driving vegetation productivity for the region, especially for tropical forests.

1. Introduction

Determining the carbon sink or source potential of ecosystems under future climate projections is of critical importance, and largely dependent on accurate understanding of the sensitivity of ecosystem-level photosynthesis to biophysical and biogeochemical change. Terrestrial gross primary production (GPP) and net primary production (NPP) quantify carbon removed from the atmosphere and converted to biomass, respectively [*Cao and Woodward*, 1998; *Melillo et al.*, 1993; *Schimel et al.*, 1997; *Tian et al.*, 2011], and serve as the foundation of all life on Earth [*Beer et al.*, 2010; *Running*, 2013]. However, the processes and mechanism driving changes in GPP and NPP over time are complex and currently not well understood.

The impact of a given climate driver on GPP/NPP can be location specific and dependent on complex interactions with multiple factors. For instance, meta-analysis from 85 studies found that experimental warming and increased precipitation generally stimulated plant growth and ecosystem C fluxes [*Z. Wu et al.*, 2011]. Yet others have found that the potential benefits of a lengthening growing season or a warming climate could be offset by increasing vegetation water stress, frequent wildfire and insect disturbances, or enhanced autumn respiration due to climate warming [*Krishnaswamy et al.*, 2014; *Piao et al.*, 2014; *Yi et al.*, 2013; *Yuan et al.*, 2014a; *Zhao and Running*, 2010].

Substantial uncertainties in both the amplitude and spatial pattern of current NPP estimates can be attributed to the above factors. For example, global GPP estimates were found to range from 105 to 177 Pg C a^{-1} over the period 1986–2005 [*Anav et al.*, 2013; *Jung et al.*, 2009, 2011; *Koffi et al.*, 2012; *Welp et al.*, 2011], whereas global NPP estimates were found to range from 37 to 83.8 Pg C a^{-1} in the 2000s [*Ito*, 2011]. To

quantify terrestrial vegetation growth more accurately and to better understand the underlying mechanisms driving trends in vegetation productivity, determination of the changes in GPP and NPP based on ecophysiological processes is required [*Ogutu et al*., 2013; *Running*, 2013]. Further regional applications of ecosystem models are desirable to clarify recent impacts of climate change and variability on the terrestrial carbon cycle.

Due to increasing availability and the spatially explicit coverage of remote sensing data over the last few decades, remote sensing-based GPP and NPP models have been widely developed and used for regional and global scale monitoring [*Gitelson et al*., 2006; *Potter*, 1999; *Potter et al*., 1993; *Prince and Goward*, 1995; *Running et al*., 2000; *Sims et al*., 2008, 2006; *C. Wu et al*., 2011; *Wu et al*., 2010a; *Xiao et al*., 2004; *Yan et al*., 2015; *Yang et al*., 2013; *Zhao et al*., 2005; *Zhao and Running*, 2010]. However, assessments of multiple models at eddy covariance flux tower sites have shown that site-level model runs performed better than region-level runs for annual and monthly fluxes largely due to spatial scale mismatches [*Raczka et al*., 2013]. In addition, none of these models were able to reproduce GPP estimates within observed uncertainties because of (1) poor responses of the models to environmental factors and (2) large uncertainties in satellite and driver data [*Raczka et al*., 2013; *Schaefer et al*., 2012; *Schwalm et al*., 2010; *Yuan et al*., 2014b].

The photosynthesis (PSN) algorithm based on satellite observations from the Moderate Resolution Imaging Spectroradiometer (MODIS) instrument provided the first 1 km global data products (MOD17) and have been widely applied in the monitoring of vegetation dynamics and ecosystem carbon flux [*Running et al*., 2004]. However, there are still large uncertainties in these products, including those introduced by upstream data inputs, biome-specific physiological parameters (i.e., Biome Properties Look-Up Table (BPLUT)), and algorithm structure [*Nightingale et al*., 2007; *Pan et al*., 2006; *Turner et al*., 2006]. MOD17 products were relatively recently upgraded from Collection 4.0 to 5.1 by improvements in the upstream data inputs [*Zhao et al*., 2005; *Zhao and Running*, 2010; *Zhao et al*., 2006]. Yet research suggested that the MODIS GPP and NPP products could be further improved through employing better driver data, higher-quality satellite observations, and recalibrated model parameters [*Kanniah et al*., 2009; *Medlyn*, 2011; *Samanta et al*., 2011; *Sjostrom et al*., 2011, 2013; *Wu et al*., 2014], which is especially necessary for regional applications. Yet few studies have validated both GPP and NPP products using localized inputs and calibrated parameters at the regional level [*Xin et al*., 2015; *Yan et al*., 2015].

For China, GPP and NPP estimates have attracted much attention, but large uncertainties still remain and limit the usefulness of these data to inform policy decisions. For instance, GPP and NPP estimates range widely from 3.90 to 12.26 Pg C and 1.43 to 3.30 Pg C, respectively (Figure 1), due to limitations in the driver data, satellite observations, and algorithm parameters [*Gao et al*., 2012; *Liu et al*., 2013]. Long-term NPP trend analyses over the period 1961–2005 did not exhibit a significant linear trend on the national scale but did show regional increasing and decreasing trends [*Q. Yuan et al*., 2014]. Relatively short-term analyses have found a declining trend in NPP over the recent decade due to extreme climate events, such as low-temperature freezing, severe drought, and/or heat waves observed for a given year [*Liu et al*., 2013; *Yuan et al*., 2016]. An accurate estimate of the spatiotemporal trends in national GPP and NPP is essential for policy decisions related to land use and, vegetation growth, and carbon flux.

Our main objective here was twofold. The first objective was to provide improved MODIS NPP products for China through the usage of localized BPLUT parameters, improved upstream input data, and an improved validation methodology based on robust networks of observed GPP and NPP estimates. The second objective was to analyze spatial patterns of NPP at the national scale and to explore regional climatic controls on NPP. The products generated in this study will be released and available online for the public, and the electronic or online resources are expected to contribute to studies of terrestrial ecosystem responses to climate change.

2. Data and Methods

2.1. The Satellite-Based NPP Algorithm (PSN)

Most satellite-based NPP models are based on the concept of light use efficiency and assume that primary production is proportional to photosynthetically active radiation (PAR) absorbed by vegetation with a light use efficiency scaling factor [*Monteith*, 1972; *Monteith and Moss*, 1977]. In this study, the satellite-based

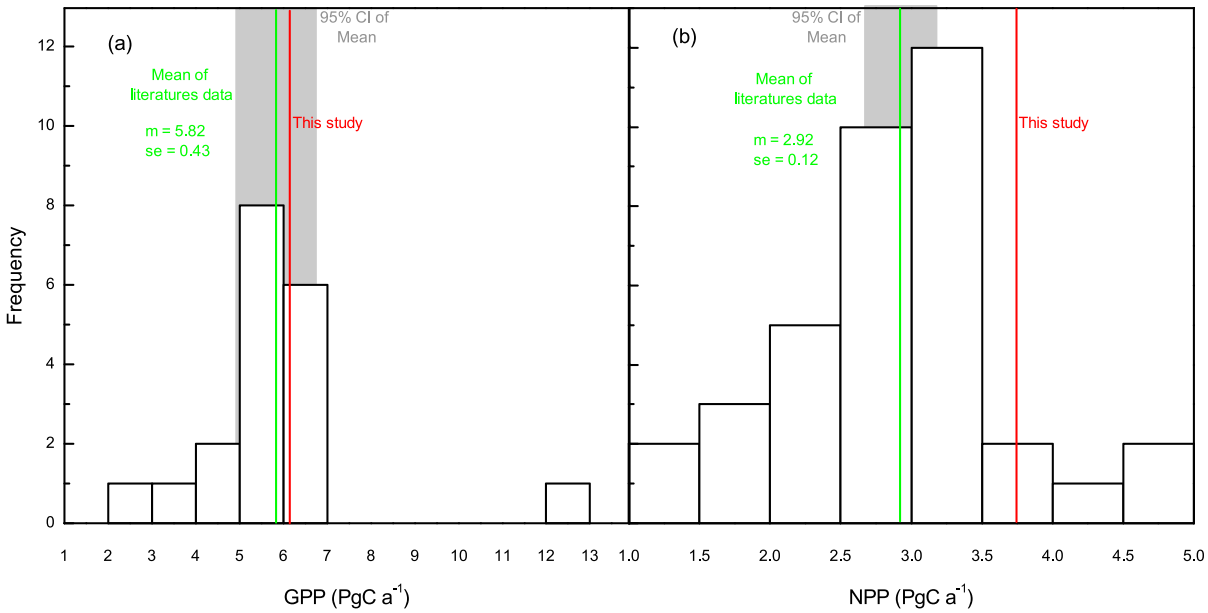

Figure 1. The frequency of the (a) GPP and (b) NPP estimates from the literature and this study across the terrestrial ecosystems of China.

NPP products were based on the MOD17 algorithm (the PSN model) that was localized by using more accurate data inputs and an optimized BPLUT based on ChinaFLUX observations. The localized NPP products generated are referred to as NPP_{CBP}. In the MOD17 algorithm, NPP is GPP minus autotrophic respiration and GPP is the product of PAR, FPAR, and actual light use efficiency (ε) (equation (1)). The ε is calculated by the biome-level maximum light use efficiency estimate (ε_{max}) and the environmental stress scalars of low-temperature ($TMIN_{scalar}$) or limited water availability (VPD_{scalar}) (equation (2)).

$$GPP = PAR \cdot FPAR \cdot \varepsilon \tag{1}$$

$$\varepsilon = \varepsilon_{max} \cdot TMIN_{scalar} \cdot VPD_{scalar} \tag{2}$$

The $TMIN_{scalar}$ and VPD_{scalar} are parameterized according to equations (3) and (4):

$$TMIN_{scalar} \begin{cases} 1 & TMIN > TMIN_{max} \\ (TMIN - TMIN_{min})/(TMIN_{max} - TMIN_{min}) & TMIN_{min} \leq TMIN \leq TMIN_{max} \\ 0 & TMIN > TMIN_{min} \end{cases} \tag{3}$$

$$VPD_{scalar} \begin{cases} 0 & VPD > VPD_{max} \\ (VPD_{max} - VPD)/(VPD_{max} - VPD_{min}) & VPD_{min} \leq VPD \leq VPD_{max} \\ 1 & VPD > VPD_{min} \end{cases} \tag{4}$$

where TMIN and VPD are the daily minimum temperature (°C) and daily mean vapor pressure deficit (Pa), $TMIN_{max}$ and VPD_{min} are the daily minimum temperature and daily mean vapor pressure deficit at which $\varepsilon = \varepsilon_{max}$, and $TMIN_{min}$ and VPD_{max} are the daily minimum temperature and average vapor pressure deficit at which $\varepsilon = 0$. These parameters were determined for each land cover type in the BPLUT.

Autotrophic respiration is separated into growth respiration and maintenance respiration (R_m). The growth respiration is assumed approximately 25% of NPP and the maintenance respiration from living wood ($g\,C\,m^{-2}\,a^{-1}$) is calculated as

$$R_m = M_l \cdot B_r \cdot Q_{10}^{\frac{T_{ave}-20}{10}} \tag{5}$$

where M_l is living biomass for leaves and fine roots ($g\,C\,m^{-2}$) and derived from leaf area index (LAI), B_r is base respiration at 20°C and determined by land cover, and Q_{10} is a respiration quotient and calculated by a temperature-acclimated equation (equation ((7)) calculated as

$$Q_{10} = 3.22 - 0.046 \cdot T_{avg} \tag{6}$$

where T_{avg} is daily average air temperature (°C). Annual NPP is calculated as

$$\mathrm{NPP} = \begin{cases} 0.8 \cdot \sum_{i=1}^{365} (\mathrm{GPP} - R_m) & \sum_{i=1}^{365} (\mathrm{GPP} - R_m) \geq 0 \\ 0 & \sum_{i=1}^{365} (\mathrm{GPP} - R_m) < 0 \end{cases} \tag{7}$$

The main data inputs into the algorithm include (1) FPAR and LAI from remote sensing; (2) daily minimum temperature, daily total incoming solar radiation, and daily mean vapor pressure deficit; (3) land cover with the classification of IGBP; and (4) a Biome Parameter Look-up Table (BPLUT) containing values of ε_{max} and other biome-specific physiological parameters for different land covers.

2.2. In Situ Observation and Ground Survey Data

2.2.1. In Situ Eddy Covariance Tower Measurements

2.2.1.1. Data for Parameterization

Eddy covariance (EC)-based daily data were applied to optimize the BPLUT in GPP estimation and evaluate the temporally filled MODIS FPAR/LAI data and surface meteorological data. ChinaFLUX provided the daily GPP and meteorological data from 2003 to 2005 at four forest sites (CBS, QYZ, DHS, and XSF), three grassland sites (HBS, XLG, and DXG), and one cropland site (YCH) (Figure 2, right). Continuous CO_2 and H_2O flux were measured using an infrared gas analyzer, and wind speed was measured using a 3-D sonic anemometer at a sampling frequency of 10 or 20 Hz at flux sites [*Yu et al*., 2014]. The data were filtered and corrected with coordinate rotation, the Webb-Pearman-Leuning correction [*Webb et al*., 1980], storage flux calculation, outlier filtering, nighttime CO_2 flux correction [*Reichstein et al*., 2005], gap filling [*Falge et al*., 2001], and net ecosystem exchange flux partitioning into GPP and ecosystem respiration [*Reichstein et al*., 2005]. Site-specific thresholds of friction velocity (u^*) were used to filter nighttime CO_2 eddy covariance flux under low atmospheric turbulence conditions by individual researchers from each site [*Yu et al*., 2014]. Data process and quality control of the EC data were conducted through the ChinaFLUX flux data processing system [*Li et al*., 2008; *Liu et al*., 2012]. Other processing details can be found in *Yu et al.* [2006], *Guan et al.* [2006], *Wen et al.* [2006], *Fu et al.* [2006], and *Zhang et al.* [2006].

2.2.1.2. Data for GPP Validation

An additional 46 site years of observed GPP data from eddy covariance towers were used for GPP validation in this study. These GPP data were previously collected by *Yu et al.* [2014, 2013]. Only sites with at least 1 year of continuous flux measurements were selected for calculating annual GPP statistics. Overall, 10 sites were included, covering six forest sites, three grassland sites, and one cropland site. See supporting information Table S1 for details regarding the site data used in this study.

2.2.1.3. Data for Assessing the Accuracy of the Meteorological Surface Data

Along with the observations from ChinaFLUX, observations from eight AsiaFLUX sites (Figure 2, right) were applied to assess the accuracy of the meteorological surface. According to *Hirata et al.* [2008], the eddy CO_2 flux was measured using the eddy covariance technique with 3-D sonic anemometer-thermometers and open- or closed-path CO_2/H_2O analyzers. Measurement systems and calculation protocols were mostly based on the EUROFLUX methodology [*Aubinet et al*., 1999; *Hirata et al*., 2008]. Details of the measurement and data process can be found in *Hirata et al.* [2008]. See supporting information Table S1 for site years, vegetation, soil, and climate characteristics of the ChinaFLUX and AsiaFLUX sites used in this study.

2.2.2. Forest Inventory Data

A database of NPP from a previous study [*Luo*, 1996] was used to validate modeled NPP. The database contained 690 NPP observations from both field and inventory plots within 17 forest types of China. Plot NPP data were estimated from the plot live biomass based on growth rates derived from stem analysis research and leaf life span. Live biomass from the inventory plots was estimated from measurements of tree height and diameter at breast height using empirical allometric regressions [*Luo et al*., 1998, 2002].

2.3. Improvements in Model Inputs and Parameterization

2.3.1. Surface Meteorology Inputs

Meteorological inputs for MODIS GPP/NPP were interpolated with observations from 836 stations in China and 345 stations in surrounding countries (Figure 2, left). The meteorological variables included daily

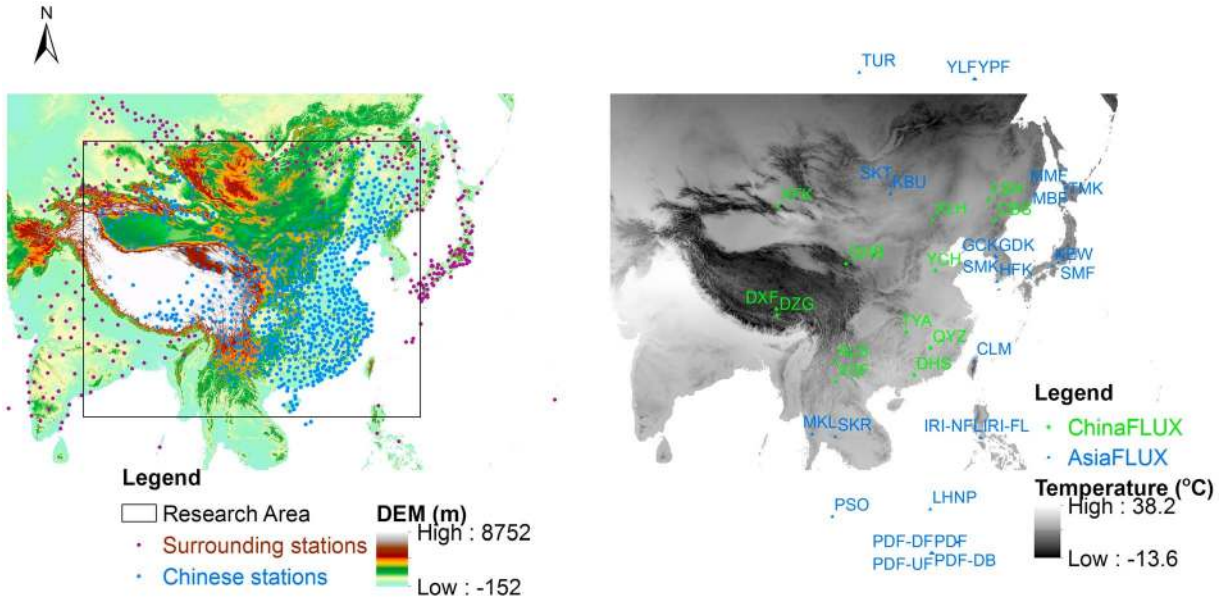

Figure 2. The (right) carbon flux sites and the (left) meteorological stations used in this study. The surface meteorological data were interpolated using observations at meteorological stations in China and surrounding countries, and a 1 km digital elevation model (DEM) from the 90 m Shuttle Radar Topographic Mission (SRTM) database v4.1 [*Farr et al*., 2007; *Rabus et al*., 2003]. The flux sites from ChinaFLUX and AsiaFLUX were used for parameter optimization and the assessment of the interpolated surface meteorological data. The temperature on 13 August 2005 from the meteorological surface data is shown as an example of the interpolation result.

minimum (T_{min}, °C), maximum (T_{max}, °C), and average (T_{avg}, °C) temperature, daily relative humidity (RHU, %), and sunshine hour (SH, h). The software of ANUSPLIN version 4.2, an algorithm based on the thin plate smoothing splines of multivariates [*Gill et al*., 2002; *Hutchinson and McIntosh*, 2000], was used to produce meteorological data at a 1 km spatial resolution and 8 day time step. One kilometer digital elevation model (DEM) data were resampled from 90 m Shuttle Radar Topographic Mission (SRTM) database v4.1 [*Farr et al*., 2007; *Rabus et al*., 2003] and used as input to the interpolation. The stations in surrounding countries were used to produce the interpolated area. The interpolated area was then clipped to a smaller research area to remove the boundary effects, especially across the Qinghai-Tibetan Plateau where there are fewer stations. The interpolated meteorological data set was referred to as CMET thereafter.

Interpolated sunshine hour data were applied to estimate daily total downward short wave solar radiation (SWrad) through the solar radiation model developed by *Bonan* [1989]. In this study the ratio of actual sunshine hours to daylight hours was applied to replace the cloud cover estimated from temperature and precipitation.

Observed climate data on ChinaFLUX and AsiaFLUX flux towers were applied as independent observations to evaluate CMET, and the coarse resolution 6-hourly NCEP/DOE II reanalysis meteorological data (NCEP2) [*Kanamitsu et al*., 2002]. The latter was interpolated to 1 km spatial resolution and applied in the MOD17 C5 products [*Zhao et al*., 2005]. Comparing to the observations, CMET and NCEP2 data both showed average R^2 above 0.95 for the temperature data. But precipitation, RHU, and SWrad of CMET were much better than that of NCEP2 with the average R^2 of values 0.70, 0.79, and 0.92 (Table 1), respectively. This indicated that the meteorological surface data interpolated from station observations was better than the smoothed coarse-scale global reanalysis data, particularly with respect to RHU (used for VPD estimation in the algorithm), and solar radiation.

2.3.2. Temporal Filling of MODIS FPAR/LAI

The latest Collection 5 1 km MODIS FPAR/LAI from 2000 through 2012 was used to calculate 1 km GPP/NPP in China. The 8 day FPAR/LAI product has a significant number of missing data due to unfavorable atmospheric conditions, such as cloudiness and heavy aerosols. These data gaps were previously filled using linear interpolation of the nearest reliable values [*Zhao et al*., 2005]. However, this method, referred to as ZHAO thereafter, may remove some within seasonal changes [*Wang et al*., 2014].

Table 1. The Comparison of the Interpolated Meteorological Data (CMET) and the NCEP/DOE II Reanalysis Data (NCEP2) Using Tower Based Observations[a]

	CMET			NCEP2		
Variable	R^2 (Mean ± SD)		Site Number	R^2 (Mean ± SD)		Site Number
T_{avg}	0.91	±0.13	14	0.97	±0.03	14
TMIN	0.93	±0.12	16	0.96	±0.03	14
SWrad	0.92	±0.06	10	0.56	±0.26	10
VPD	0.77	±0.22	7	0.51	±0.22	4

[a]The CMET used in this study and NCEP2 used in MOD17 C5 products were evaluated using multiple correlation coefficients (R^2) from linear regressions with the corresponding variables observed on the eddy covariance towers from ChinaFLUX and AsiaFLUX.

The ZHAO method and other methods were evaluated with observed GPP from ChinaFLUX sites. The other methods included the adaptive Savitzky-Golay (SG) method in TIMESAT software [*Jönsson and Eklundh*, 2004], and the locally adjusted cubic-spline capping (LACC) method [*Chen et al*., 2006]. Multiple correlation coefficients (R^2) of linear regression were analyzed between the observed GPP and FPAR filled by the different methods or the FPAR unfilled on the ChinaFLUX sites. Over all sites except for tropical forest, the average R^2 was 0.67 for the MOD15A2 raw data and 0.82, 0.80, and 0.76 for the filling methods of SG, ZHAO, and LACC, respectively. Across tropical forest sites, all R^2 values were lower than 0.25 (Table 2). Even though performance was limited for all methods in tropical forest sites, the comparison showed that the SG method was better than the others.

Based on the above analysis, the FPAR and LAI data were reprocessed using the TIMESAT software [*Jönsson and Eklundh*, 2004]. Although the quality control and assessments information is useful and considered in the MOD17 algorithm [*Zhao et al*., 2005], it was not considered in the application of the SG method in this study since the SG method is effective at removing noise from time series data. Prior to late February 2000, FPAR/LAI is not available, and these missing gaps were filled by averaging the corresponding 8 day reliable FPAR/LAI from 2001 to 2003, in order to calculate a complete annual MODIS GPP and NPP data set for the year 2000.

2.3.3. Land Cover Information Improvement

The MODIS land cover product (MOD12) has changed considerably from Collections 4 to 5. The Collection 5 version of MCD12 has increased spatial resolution and differences in its input data and classification algorithm relative to Collection 4. With respect to overall Collection 5 accuracy, about 75% of classifications were correct based on a global cross-validation analysis [*Keith et al*., 2012]. However, an accuracy assessment of MCD12 in China in 2005 indicated that the Kappa coefficient [*Foody*, 2002] was only 0.44 (Table 3).

A land use and cover product based on Landsat data in 2005 (LUC05) was used to improve the MODIS land cover product (Figure 3a) as inputs to the NPP algorithm. The LUC05 was from China's Land-Use/cover Dataset (CLUDs) that was interpreted from Landsat Thematic Mapper/Enhanced Thematic Mapper on the scale of 1:100,000 [*Liu et al*., 2014, 2003a, 2005, 2010, 2003b]. The LUC05 has higher accuracy but the different classification scheme with the MODIS product. Therefore, the method suggested by *Feng et al*. [2007] was applied to improve the accuracy of the MCD12. First, a new data set was produced by assigning the class codes of MCD12 according to the land use type in LUC05. Second, the forest type in the new data was classified according to the

Table 2. The Multiple Correlation Coefficients (R^2) of Linear Regression Analyzed Between the Observed GPP and the FPAR unFilled (UnFilled) and the FPAR Filled by the Methods of the Adaptive Savitzky-Golay (SG) Method in TIMESAT Software [*Jönsson and Eklundh*, 2004], the Linear Interpolation (ZHAO) of the Nearest Reliable Values [*Zhao et al*., 2005], and the Locally Adjusted Cubic-Spline Capping (LACC) [*Chen et al*., 2006] on the ChinaFLUX Sites

Sites	Vegetation Types	Unfilled	SG	ZHAO	LACC
YCH	Crop	0.60	0.80	0.78	0.75
XLG	Temperate grass	0.70	0.70	0.68	0.59
HBG	Alpine grass	0.86	0.91	0.89	0.91
DXG	Alpine grass	0.70	0.87	0.84	0.78
CBS	Temperate forest	0.66	0.95	0.93	0.90
QYZ	Subtropical forest	0.52	0.68	0.66	0.63
DHS	Tropical forest	0.12	0.03	0.01	0.19
XSF	Tropical forest	0.01	0.00	0.25	0.01

Table 3. The Optimized Parameters Used in the Satellite-Based GPP/NPP Algorithm ($MOD17_{CBP}$) Based on Localized Data in China

Vegetation Classification Code	Vegetation Classification	$TMIN_{min}$ (°C)	$TMIN_{max}$ (°C)	VPD_{min} (Pa)	VPD_{max} (Pa)	ε_{max} (g C MJ^{-1})
1	ENF	−6.87	4.87	241	3834	1.539
2	EBF	−1.48	23.70	296	2673	2.201
3	DNF	−8.00	10.44	650	2300	1.086
4	DBF	−6.00	9.94	650	1650	1.165
5	MF	−10.27	20.76	192	2466	1.776
6	CShrub	−8.00	8.61	650	4700	1.281
7	OShrub	−8.00	8.80	650	4800	0.841
8	WSavannas	−8.00	11.39	650	3200	1.239
9	Savannas	−8.00	11.39	650	3100	1.206
10	Grass	−3.04	9.99	390	2743	0.672
12	Crop	−3.97	8.48	409	4752	1.831

forest subtype in MCD12. Third, if a pixel was classified as forest in the new data but not in MCD12, the forest type of the nearest neighbor of the pixel in MCD12 was used. The final classification was referred to as $MCD12_{ADJ}$ and shown in Figure 3b.

In the new $MCD12_{ADJ}$ land cover classification, forest, cropland and grassland cover 19%, 25%, and 43%, respectively, of total vegetated area in China (Figure 3b), compared to 21%, 27%, and 32% in the old version (MCD12, Figure 3a). The old version of MCD12 data overestimated forest area and underestimated the grasslands with close estimation of cropland.

2.3.4. Parameter Optimization

Using in situ daily tower GPP measurements, the Markov Chain Monte Carlo (MCMC) method was applied to optimize the five parameters in the GPP algorithm: ε_{max}, $TMIN_{min}$, $TMIN_{max}$, VPD_{min}, and VPD_{max}, as shown in equation 2–4. The MCMC (Bayesian analysis) method derives the data-dependent probability distribution of the parameters by using the function of the Delayed Rejection and Adaptive Metropolis (DRAM) procedure [*Haario et al.*, 2006, 2001]. The lower and upper bounds of the parameters were determined from parameters in Collection 5 of the MOD17 products. The 8 day mean daily minimum temperature, daily total incoming solar radiation, and vapor pressure deficit were calculated from observations at the ChinaFLUX towers (supporting information Table S1). Remote sensed FPAR and LAI data were extracted at each flux tower site using an average of a 3 × 3 1 km pixel window centered on the site. Both

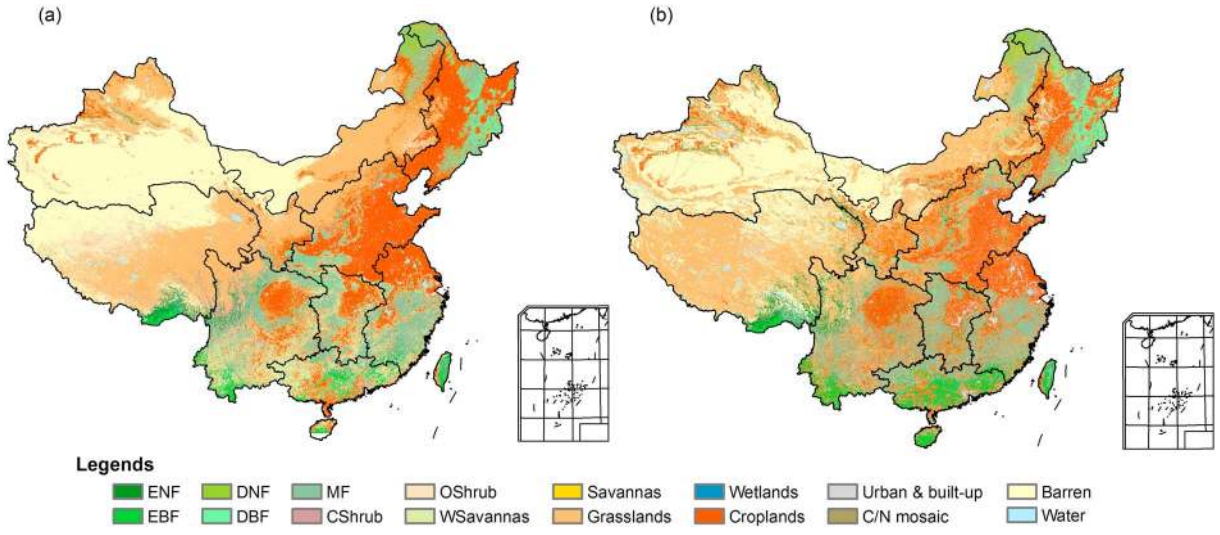

Figure 3. The improvements in land cover and land use classification in this study. (a) MODIS land cover (MCD12Q1) of Collection 5 with IGBP classification in 2005. (b) The improved MCD12Q1 ($MCD12_{ADJ}$) based on the land cover and use classification based on Landsat data in China in 2005 and the MCD12Q1.

meteorological and remote sensing data were used as the inputs for the parameters optimization. The MCMC optimization was conducted by minimizing the root-mean-square difference (RMSD) between site observed and $MOD17_{CBP}$ estimated GPP.

The final optimized parameters showed that temperature and VPD thresholds on photosynthesis and ε_{max} were very different from the default values in $MOD17_{C55}$ (Table 3). The optimized ε_{max} values were 1.539 g C MJ^{-1}, 2.201 g C MJ^{-1}, 1.051 g C MJ^{-1}, and 1.831 g C MJ^{-1} for evergreen needleleaf forest, evergreen broadleaf forest, mixed forest and crop, which were more than 60% larger than the default values used in the $MOD17_{C55}$ product. The optimized ε_{max} values for grassland was 0.672 g C MJ^{-1}, which was smaller than 0.860 g C MJ^{-1} fixed for grassland in the $MOD17_{C55}$.

2.4. Analysis

2.4.1. Results Validation

Considering the footprint issues of flux towers, many studies used a 3×3 1 km pixel window around the flux tower for validation to improve spatial agreement [*Friend et al*., 2007; *C. Wu et al*., 2011; *Wu et al*., 2010b]. We followed that protocol here and extracted data using a 3×3 1 km pixel window centered on the flux tower site for GPP and the sample plot for NPP. The averaged values of the 3×3 pixel window were calculated and compared with ground data. The 1 km global MODIS GPP/NPP products (MOD17A3 Collection 5.5, here denoted as $MOD17_{C55}$) were applied to compare and assess the improvements in the $MOD17_{CBP}$ products. The $MOD17_{C55}$ data during 2000–2012 were produced by the Numerical Terradynamic Simulation Group (http://www.ntsg.umt.edu/). $MOD17_{C55}$ used coarse resolution meteorological daily data input from the NCEP/DOE II reanalysis (NCEP2) [*Kanamitsu et al*., 2002], and linear-filling based MODIS FPAR/LAI as inputs [*Zhao et al*., 2005; *Zhao and Running*, 2010; *Zhao et al*., 2006].

2.4.2. Regional Climate Control on NPP

A multiple linear regression method was applied to analyze the influence of climate variables on the interannual variability of NPP as the following equation:

$$y = b_t \cdot x_t \cdot b_p \cdot x_p \cdot + b_r \cdot x_r + \varepsilon \tag{8}$$

where y was the NPP and x_t, x_p, and x_r were climate variables including temperature, precipitation, and solar radiation, respectively. All variables (including x and y) were normalized as below:

$$z_i = \frac{x_i - \overline{x}}{s} \tag{9}$$

where x_i was the climate variable or NPP in the ith year and $\overline{x}$ and s were the mean and the standard deviation of the time series x, respectively. Therefore, the regression coefficients b_t, b_p, and b_r represent the contribution of each climate variable to NPP.

3. Results

3.1. Accuracy Assessment of GPP/NPP Estimation

The accuracy of $MOD17_{CBP}$ GPP/NPP estimates were assessed through (1) comparison of $MOD17_{CBP}$ GPP estimates against observed GPP data across a network of eddy flux towers and (2) comparison of $MOD17_{CBP}$ NPP estimates against distributed in situ NPP measurements. Compared with observed GPP data collected from the peer-reviewed literature, $MOD17_{CBP}$ GPP had an R^2 of 0.90 (Figure 4a), while the R^2 value was 0.76 for $MOD17_{C55}$ (Figure 4b). The relative GPP RMSE values decreased to 16.2% for $MOD17_{CBP}$ compared to 24.7% in $MOD17_{C55}$. Validation analysis suggested that the localized inputs and parameters optimization ($MOD17_{CBP}$) greatly improved the performance of GPP simulation by increasing the R^2 by 18.1% and decreasing the relative RMSE by 34.2% compared with that of $MOD17_{C55}$.

$MOD17_{CBP}$ NPP was significantly correlated with in situ NPP measurements (Figures 4c and 4d). The R^2 value for $MOD17_{CBP}$ was 0.71 compared to 0.64 for $MOD17_{C55}$. Further, the relative RMSEs for $MOD17_{CBP}$ and $MOD17_{C55}$ were 21.0% and 32.7%, respectively. Validation analysis demonstrated that the localized inputs and parameters optimization ($MOD17_{CBP}$) greatly improved the performance of NPP simulation by increasing the R^2 by 10.9% and decreasing the relative RMSE by 35.8% compared with that of $MOD17_{C55}$.

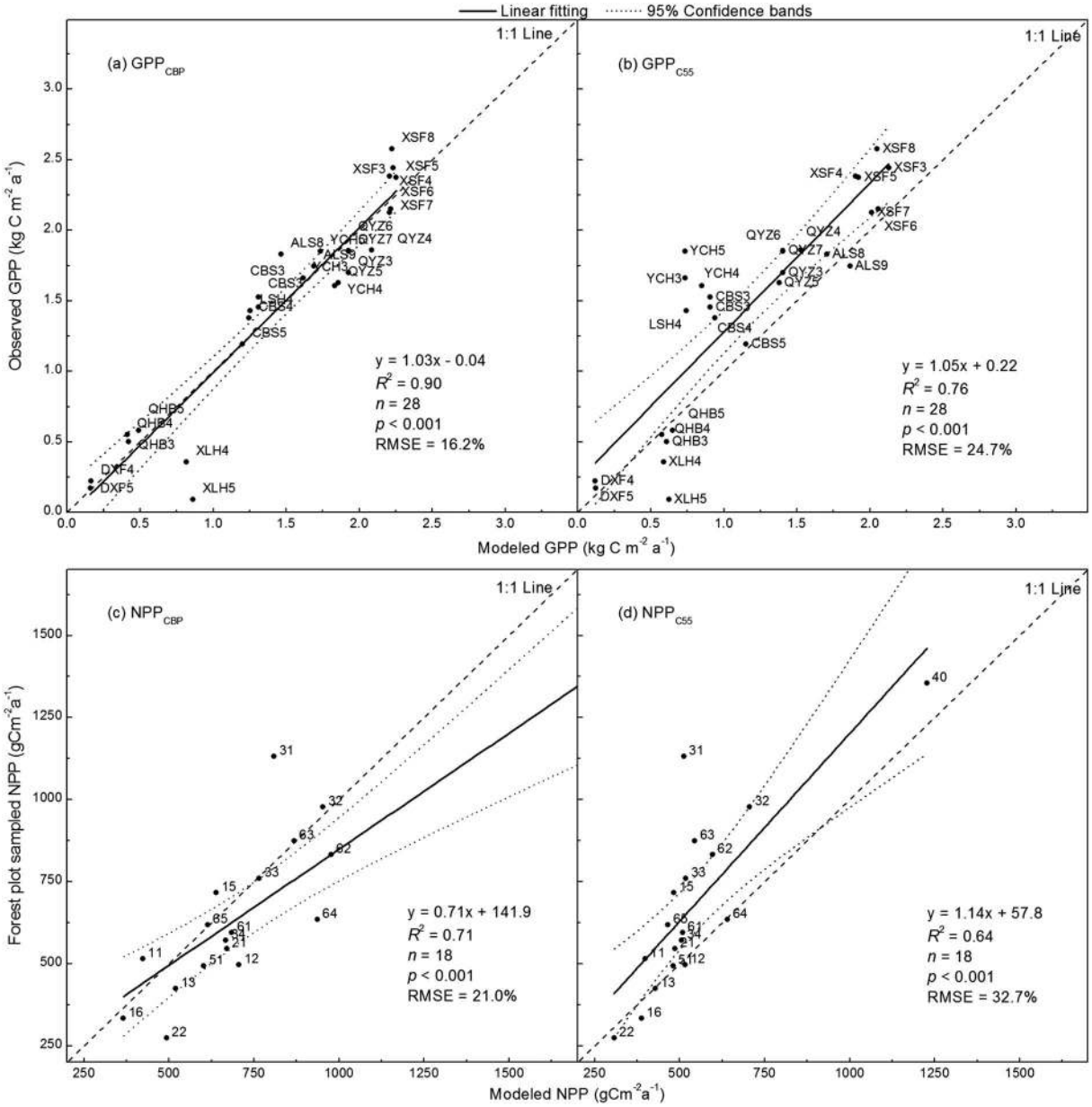

Figure 4. The (a, b) GPP and (c, d) NPP from MOD17CBP (Figures 4a and 4c) and MOD17 Collection 5.5 (Figures 4b and 4d) compared with the EC tower based GPP and NPP, respectively. The in situ GPP were multiple site year observations from ChinaFlux, and the labels are given with the combination of the site name and the year of data acquisition. The in situ NPP was averaged for each forest type from forest inventory data.

The national total GPP from the $MOD17_{CBP}$ was close to the average value (5.82 ± 0.43 Pg C a^{-1}) from 19 existing studies (Figure 1a), whereas total NPP was ~28.3% increased relative to the average NPP from 37 existing NPP data sets (2.92 ± 0.12 Pg C a^{-1}) (Figure 1b). The $MOD17_{CBP}$ GPP was especially close to that of the EC-LUE model (6.04 Pg C a^{-1}) during 2000–2009 [*Li et al.*, 2013]. GPP was greater than that of $MOD17_{C55}$ (5.10 Pg C a^{-1}) during 2000–2012 [*Zhao and Running*, 2010] and the predicted GPP of 5.38 Pg C a^{-1} in 2000–2007 from *Yuan et al.* [2010].

3.2. Spatial Pattern of NPP in China

According to $MOD17_{CBP}$, terrestrial ecosystems in China had a total NPP of 3.73 Pg C a^{-1} (Pg C $a^{-1} = 10^{15}$ g C yr^{-1}) during 2000–2012. Spatial patterns of NPP are shown in Figure 5. Higher NPP values were distributed over the South, Central, and Southwest China where evergreen forests are the dominant

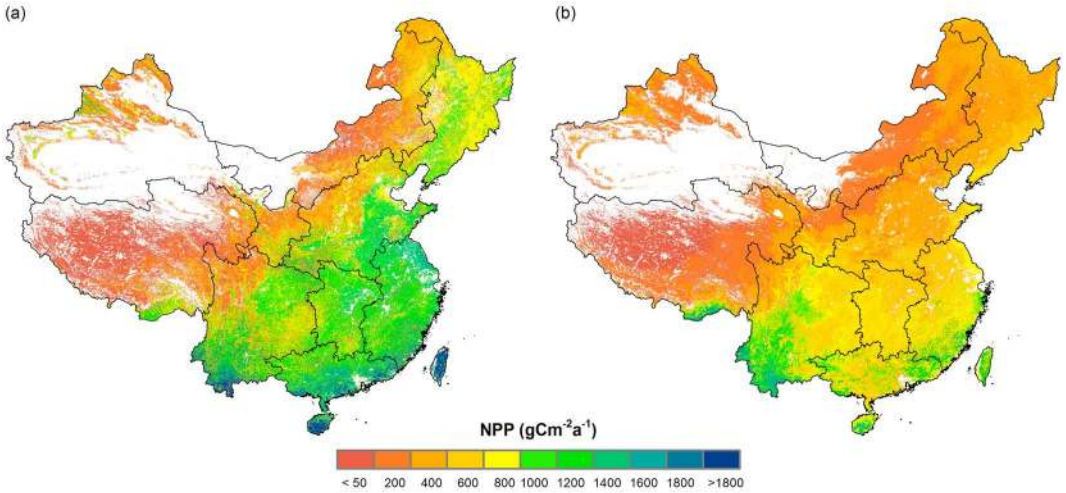

Figure 5. The spatial pattern of NPP from CBP (NPP_{CBP}) and MOD17 Collection 5.5 (NPP_{C55}) for terrestrial ecosystems in China.

vegetation type with NPP values above 700 g C m^{-2} a^{-1}. Eastern Inner Mongolia, Northwest China, and Qinghai-Tibetan plateau, characterized by grasslands and desert area, showed lower NPP under 200 g C m^{-2} a^{-1}. The NPP values over the temperate forests and croplands of Northeast and North China were about 600 g C m^{-2} a^{-1}, respectively.

Overall, regional NPP estimates were significantly variable, with NPP in Southwest China the highest and NPP in Qinghai-Tibetan plateau the lowest (Figure 5). Southwest China's total NPP of 0.80 Pg C a^{-1} represents 21.3% of China's total NPP. Relatively high NPP in this region is likely due to a warm and wet climate and greater forest cover. East, North, Northeast, and South China have a relatively medium level of NPP, which ranged from 0.46 to 0.61 Pg C a^{-1} and accounted for 12.4 to 16.3% of China's total terrestrial NPP, respectively. Northwest China and the Qinghai-Tibetan Plateau are at the lower level of NPP estimates with a total NPP less than 0.18 Pg C a^{-1} (4.8%), due in part to the harsh climate and grassland dominated landscape.

3.3. Temporal Trend of NPP and Climatic Controls

There were large variations in NPP temporal trends across the country from 2000 to 2012 (Figure 6a). NPP increased by 2.02 Tg C a^{-1} (or 7.9 ± 7.8 g C m^{-2} a^{-1} mean ± standard deviation, significant level $p < 0.05$) over 9.4% of the vegetated land in China while it decreased by 6.67 Tg C a^{-1} (or 17.4 ± 9.3 g C m^{-2} a^{-1}, $p < 0.05$) over 8.1% of the vegetated land, mostly in the productive forest areas, which resulted in an overall decreasing trend in NPP of 4.65 Tg C a^{-1} or 0.13% a^{-1}.

The trend of NPP greatly varied with climate and also by region. Overall, the NPP of grasslands and croplands increased by 0.41 Tg C a^{-1} and 0.32 Tg C a^{-1}, respectively, while NPP of forests decreased by 5.38 Tg C a^{-1}. The increasing trend mainly occurred in the croplands of North China (0.52 Tg C a^{-1}), Northwest China (0.50 Tg C a^{-1}), and Northeast China (0.33 Tg C a^{-1}), and the forests of Northeast China (0.28 Tg C a^{-1}). These areas accounted for 95.6% of the increasing trend of NPP in the whole country (Figure 7). The decreasing trend was seen in almost all the forest areas in South China. Specifically, the forest NPP decreased by 1.81 Tg C a^{-1}, 1.42 Tg C a^{-1}, 1.02 Tg C a^{-1}, and 0.99 Tg C a^{-1} in South China, Central China, Southeast China, and Southwest China, respectively. These areas accounted for 78.5% of the decreasing NPP trend for the whole country (Figure 7). On the Qinghai-Tibetan Plateau, the grasslands and croplands showed increasing NPP trends of 0.31 Tg C a^{-1} and 0.05 Tg C a^{-1}, respectively, whereas forests in the region showed a decreasing NPP trend of 0.52 Tg C a^{-1}, resulting in a total decreasing trend in the plateau of 0.16 Tg C a^{-1}. The results clearly suggest that NPP in North China increased for cropland and grassland but decreased for forests in South China over the period of this study.

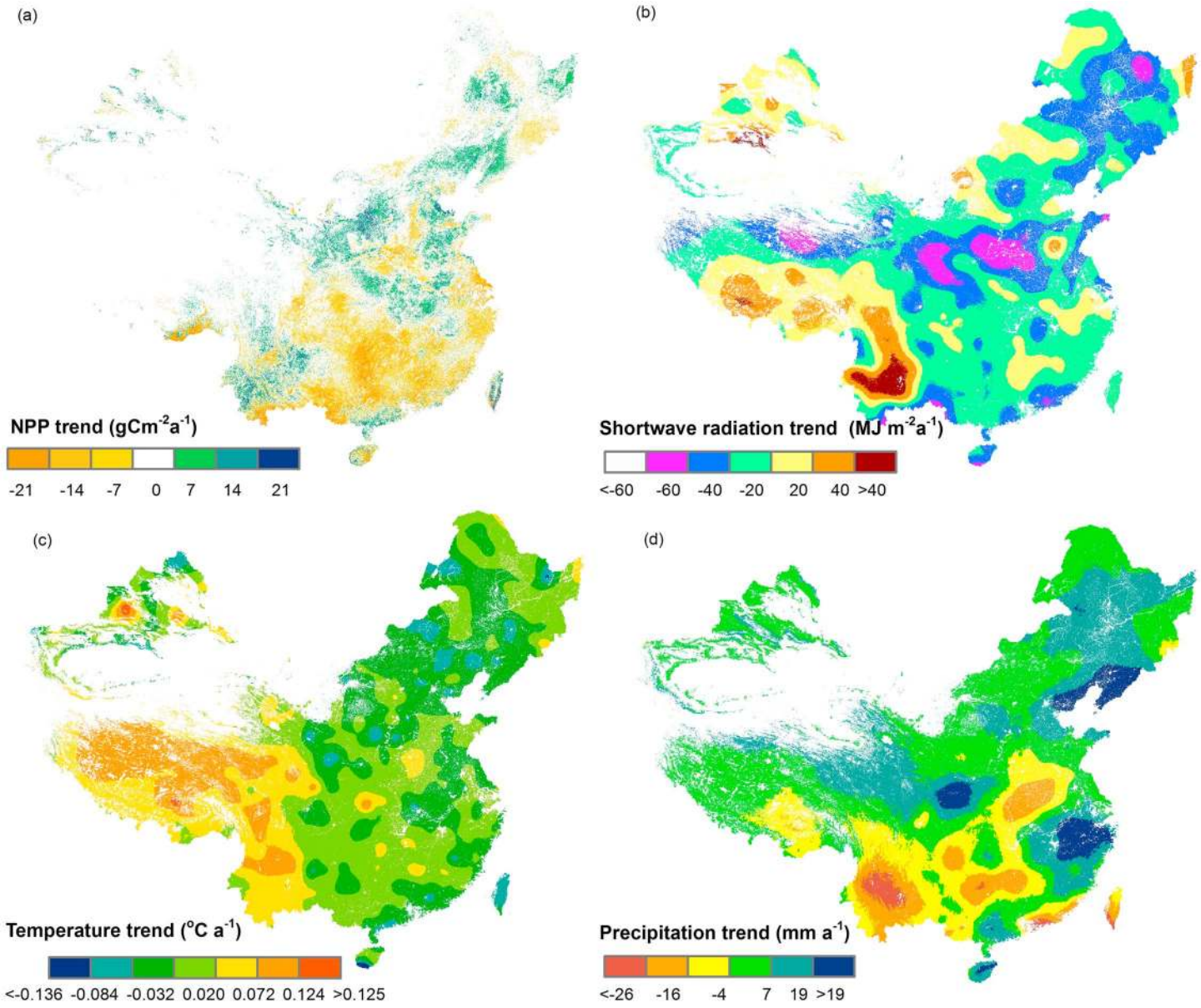

Figure 6. Spatial distribution of trends in (a) NPP from $MOD17_{CBP}$ (NPP_{CBP}) and (b) shortwave solar radiation (SWRad), (c) annual mean temperature (AMT) ,and (d) annual total precipitation (ATP) from 2000 to 2012.

3.4. Impacts From Climate Change on NPP Trend

In 2000–2012, trends in temperature, precipitation, and SWRad showed remarkable regional differences (Figure 6 and Table 4). A warming trend was found over Qinghai-Tibetan Plateau ($p = 0.07$) and Southwest China ($p = 0.32$), and a weak cool trend in other areas ($p > 0.05$). Meanwhile, a wetting trend was found in Northeast China ($p = 0.01$), Inner Mongolia ($p = 0.07$), and Northeast China ($p = 0.05$) while a drying trend on Qinghai-Tibetan Plateau and in Southwest China ($p = 0.10$). Solar shortwave radiation (SWRad) showed an increasing trend in Southwest China ($p = 0.82$) and a decreasing trend in other regions ($p > 0.05$).

The observed trends in NPP can be well explained by changes in precipitation, temperature, and SWRad. In fact, these three variables together were found to explain over 66% of the increasing trend of NPP in North China and 55–73% of the decreasing trend in NPP in South China (Table 4). Over North China, vegetation is more sensitive to changes in precipitation, and increasing NPP can be explained by a weak increase in precipitation with R^2 values of 0.41 ($p = 0.02$), 0.69 ($p < 0.01$), 0.18 ($p = 0.15$), and 0.45 ($p = 0.01$) for Northwest

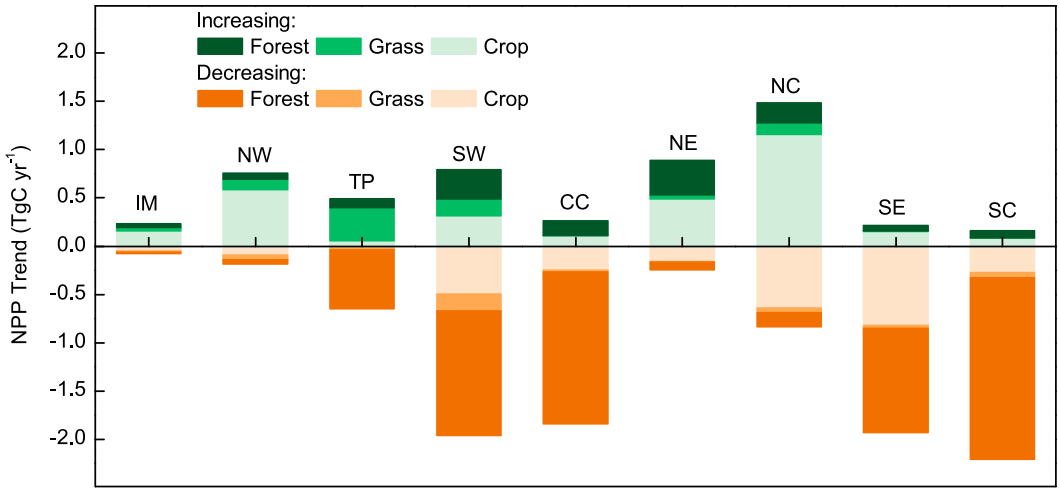

Figure 7. NPP trend of each main vegetation type in the nine regions in China from 2000 to 2012.

China, Inner Mongolia, Northeast China, and North China, respectively. On the Qinghai-Tibetan Plateau, precipitation, temperature, and SWRad together controlled the interannual variation of grassland NPP and the R^2 values were 0.53, 0.51, and 0.48, respectively, with a significant level $p < 0.01$, while temperature played an important role in forest NPP variation with a R^2 of 0.61 ($p = 0.002$), which was mainly distributed in the southern part of the plateau.

Over South China, the interannual variability of NPP was best explained by SWRad changes instead of changes in precipitation. The R^2 between the standardized NPP and SWRad was 0.29 ($p = 0.06$), 0.29 ($p = 0.06$), 0.59 ($p < 0.01$), and 0.46 ($p = 0.01$) for Southwest China, Central China, South China, and Southeast China, respectively, while the R^2 between NPP and precipitation was less than 0.13 ($p > 0.05$) for these same regions. For Southwest China, drought years occurred in 2006, 2011, and 2009 in which precipitation was 1.8, 1.5, and 1.3 times less than the standard deviation (SD) of the average from 2000 to 2012. Yet minimum NPP (11.3 Tg C a^{-1}), which was 1.84 times less than the SD of the average from 2000 to 2012, occurred in 2012, not during the three drought years. NPP was better correlated with precipitation from the previous year ($R^2 = 0.23$) compared to precipitation data from the same year ($R^2 = 0.13$). Despite the lagged response of NPP to precipitation, NPP was still more sensitive to SWRad than to precipitation. The ratios of the standardized regression coefficient of the radiation and precipitation terms were found to range

Table 4. The 2000–2012 Interannual Trends of NPP and Related Climate Variables for the Dominant Vegetation in the Each Region of China[a]

Region	Dominant Vegetation	Area[b] (%)	NPP Trend (Tg C a^{-1})	TEM Trend (°C $10a^{-1}$)		PRCP Trend (mm a^{-1})		SWRad Trend (MJ m^{-2} a^{-1})		NPP = $b_{TEM} + b_{PRCP} + b_{SWR} + \varepsilon$			
										b_{TEM}	b_{PRCP}	b_{SWR}	R^2
NW	Grass	6.71	0.57	−0.17	(0.54)	3.68	(0.01)	−1.26	(0.51)	0.03	0.43	0.19	0.68
IM	Grass	1.62	0.16	−0.46	(0.22)	5.35	(0.07)	−5.16	(0.45)	−0.10	0.81	0.25	0.70
NE	Forest	3.43	0.65	−0.34	(0.47)	10.21	(0.05)	−16.63	(0.12)	−0.06	0.41	0.58	0.66
NC	Crop	7.65	0.65	−0.33	(0.22)	3.71	(0.53)	−19.08	(0.07)	0.02	0.45	0.57	0.66
TP	Grass	36.89	−0.16	0.60	(0.07)	3.63	(0.10)	−2.90	(0.54)	0.52	0.36	0.06	0.70
SW	Forest	22.69	−1.17	0.25	(0.32)	−8.24	(0.10)	2.21	(0.82)	0.04	0.29	0.49	0.70
CC	Forest	6.63	−1.58	−0.13	(0.62)	−7.40	(0.57)	−6.69	(0.51)	−0.28	0.65	0.93	0.66
SC	Forest	9.95	−2.05	−0.37	(0.17)	−10.40	(0.56)	−18.00	(0.29)	−0.08	0.57	0.96	0.69
SE	Forest	4.44	−1.72	−0.31	(0.18)	6.36	(0.63)	−6.55	(0.60)	0.32	0.29	0.66	0.68
Total		17.5[c]		−4.65	(0.39)	1.47	(0.40)	−8.64	(0.39)	0.19	0.40	0.40	0.69

[a]The interannual trends of NPP were analyzed for pixels with a significance level $p < 0.05$. The climate variables analyzed were temperature (TEM), precipitation (PRCP), and solar shortwave radiation (SWRad). Linear trend significance levels are in brackets. Multiple linear regressions were applied in the impacts analysis of climate change on NPP and given with the regression coefficient of temperature (b_{TEM}), precipitation (b_{PRCP}), and solar shortwave radiation (b_{SWR}), and correlation coefficient (R^2).
[b]The area is the total area where NPP significantly increased or decreased in vegetated area in each region.
[c]This percent is the area where NPP significantly increased or decreased in the vegetated area in whole country.

from 1.43 to 2.28 across southern China (Table 4), indicating that NPP was significantly more sensitive to radiation relative to precipitation. Partitioning the decreasing NPP trend for Southern forests of 6.52 Tg C a^{-1}, we find drought played a minor role decreasing NPP by 1.17 Tg C or 18% of the total trend, whereas radiation was the primary driver decreasing NPP by 5.35 Tg C or 82% of the total trend, as showed in Table 4.

4. Discussion

4.1. Uncertainties in NPP Estimations

4.1.1. Model Improvements in This Study

We improved GPP and NPP estimates for China for the period 2000–2012 in three key ways. First, we utilized high-resolution localized meteorological driver data. The $MOD17_{C5}$ uses climate data from NCEP2, while the coarse spatial resolution of these data has been shown to be a dominant factor driving uncertainties in global GPP and NPP products [*Betts et al*., 2006; *Sjostrom et al*., 2013; *Zhao et al*., 2006]. In particular, the SWRad data have been shown to disproportionately contribute to uncertainties due to relatively limited observations of in situ incoming radiation [*Kalnay et al*., 1996; *Yi et al*., 2011]. Notably, SWRad data were found to have relatively large uncertainties and errors for south China in particular [*Cai et al*., 2014]. In this study, we used sunshine duration-based SWRad estimates which were suggested by [*Yang et al*., 2006] and demonstrated by [*Li et al*., 2015] to be a more accurate method for deriving PAR. Second, we utilized improved noise removal in the MOD15A2 FPAR/LAI data. Similar noise removal methods have been previously demonstrated effective for the improved estimation of net ecosystem production (NEP) [*Wang et al*., 2011], and the performance of these methods have been verified by many previous analysis [*Lin et al*., 2012; *Nightingale et al*., 2009; *Wang et al*., 2014; *Zhang et al*., 2009, 2012]. Third, we utilized a more accurate representation of land cover being an important factor influencing the uncertainty in the biome-specific parameters. A previous study showed that the uncertainty from land cover classification can account for relatively large errors in GPP (−15.8% to 8.8%), NPP (−5.6% to 20.0%), and NEP (−14.8% to 67%) [*Quaife et al*., 2008]. To achieve this, we combined the MODIS land cover products with more detailed vegetation classifications, and the Landsat-based land cover products with higher resolution and more accurate [*Liu et al*., 2014, 2003a, 2005, 2010, 2003b].

4.1.2. Parameters Optimization

The parameters in the GPP algorithm were optimized through the observed GPP from ChinaFlux, which improved the accuracy of GPP estimation at sites. Potential light use efficiency (ε_{max}) was found to be one of most important parameters influencing GPP estimates and was considered to be underestimated by $MOD17_{C55}$ [*Liu et al*., 2015]. In this study, the optimized values were 1.839 g C MJ^{-1}, 1.831 g C MJ^{-1}, and 0.672 g C MJ^{-1} for forests, crops, and grass, respectively, which were in the range of 0.796–2.53 g C MJ^{-1}, 1.056–3.864 g C MJ^{-1}, and 0.199–1.8818 g C MJ^{-1} for forests, cropland, and grassland, respectively [*J. Chen et al*., 2009; *Zhang et al*., 2008]. However, ε_{max} was found to be spatially heterogeneous within biome types [*B. Chen et al*., 2009; *Madani et al*., 2014]. But the observed GPP in cropland was available only from one site in this study and the optimized parameter was applied to regional scale, which would be the main reason of the overestimated NPP. Therefore, in the future, the spatial estimation of LUE using remote sensing is expected to improve global ecosystem productivity estimation.

A vapor pressure deficit (VPD)-based stressor was a widely criticized problem in the MOD17 algorithm and previous studies suggested that a soil moisture based water stress should be included in the algorithm [*Kanniah et al*., 2009; *Leuning et al*., 2005; *Mu et al*., 2007; *Pan et al*., 2006; *Yan et al*., 2015]. However, analyses have shown that models that do not directly consider soil moisture can still capture the impacts of drought on GPP [*He et al*., 2013; *Wagle et al*., 2014]. We may infer that the VPD based water stressor is applicable in this study.

4.1.3. Model Improvements in the Future

To decrease uncertainties from inputs and model structure, a fundamental improvement relies on the developments of next generation satellite sensors. The Soil Moisture Active Passive (SMAP) mission, for example, could provide accurate global mapping of freeze-thaw state and surface soil moisture with 2–3 day temporal fidelity and enhanced (≤9 km) spatial resolution [*Yi et al*., 2011]. New space-based observations of chlorophyll fluorescence have been demonstrated to enable an accurate, global, and time-resolved measurement of crop photosynthesis and ecosystem light use efficiency [*Guanter et al*., 2014].

4.2. The Trend of NPP and Climate Impact

4.2.1. The Trend of NPP

We found an overall decrease of NPP of 4.65 Tg C a^{-1} or 0.13% a^{-1} for China from 2000 to 2012, with increases in NPP over North China more than offset by decreases in NPP over the more productive forested regions of South China. These findings are consistent with long-term trend analyses, which have suggested that the NPP for the whole region of China increased over the past two decades, but switched to a decreasing trend this decade [*Cao et al*., 2003]. Further, these findings are consistent with emerging evidence that the potential benefits from a lengthening growing season and warming climate could be offset by increasing vegetation water stress, frequent wildfire and insect disturbances, or enhanced autumn respiration due to climate warming [*Krishnaswamy et al*., 2014; *Piao et al*., 2014; *Yi et al*., 2013; *Yuan et al*., 2014a; *Zhao and Running*, 2010]. For China, the impacts of climate changes on terrestrial ecosystems seem to have switched from positive to negative effects at the national scale, although variability by region is significant.

4.2.2. Impacts From Climate Change

Dominant drivers of NPP include the fertilization effects of rising atmospheric CO_2 concentration, atmospheric nitrogen deposition, damaging ozone concentrations, land cover and land use changes, and climate changes [*Piao et al*., 2015; *Smith et al*., 2016; *Tian et al*., 2011; *Xiao et al*., 2015]. In this study, we focused on the influence of climate drivers and found that climate was a dominant factor driving NPP across China from 2000 to 2012 ($R^2 = 0.66$–0.70) (Table 4). This finding in turn suggests that about 30% of the trend in NPP could be attributed to others factors, such as land use changes including of afforestation and reforestation, which should be included in future research efforts [*Piao et al*., 2015; *Tian et al*., 2011; *Zhang et al*., 2014].

Across South China, a region affected by the East Asian monsoon, the growth of vegetation can be constrained by solar radiation due to the frequent presence of heavy clouds [*Zhang et al*., 2014; *Zhao et al*., 2001]. In this study, the effects of solar radiation and precipitation were both positive; however, NPP was more sensitive to radiation relative to precipitation. Thus, the decreasing trend in NPP over South China was most likely driven by a decreasing trend in shortwave radiation (SWRad). These findings are supported by recent model simulation experiments, and the provincial statistics approach indicated solar radiation as the leading climate factor in the trend of vegetation growth on the regional scale in China [*Xiao et al*., 2015; *Zhang et al*., 2014]. Over the recent 30 years, increasing air pollution and atmospheric concentrations of aerosols have potentially resulted in reductions in direct radiation across China, whereas diffuse radiation may have increased [*Fu et al*., 2015; *Ren et al*., 2014]. Our results indicate that these changes could have contributed to observed reductions in vegetation productivity over South China. Conversely, the effects of increasing diffuse radiation on NPP remain relatively unknown and a source of uncertainty in our analysis. Models have been recently developed to account for such effects, including the cloudiness index light use efficiency (CI-LUE) model [*Wang et al*., 2015], and a two-leaf light use efficiency (TL-LUE) model [*He et al*., 2013]. However, the photosynthesis mechanism under diffuse radiation conditions, especially in tropical forests, requires further investigation and should be a priority focus of future research efforts.

5. Conclusions

In this study, we introduce an improved NPP algorithm for the region of China that used regional parameterization, high-resolution meteorological data, and Landsat-based land cover products. We found our improved NPP algorithm significantly reduced bias in NPP estimates, suggesting researches should exercise caution with regional application of global products. We found an overall reduction in NPP of 4.65 Tg C a^{-1} for the region of China from 2000 to 2012, with increases in NPP over North China more than offset by decreases in NPP over the more productive forested regions of South China. Climate, precipitation, temperature, and solar radiation, together, play a dominant role ($>$ 70%) in the interannual variability of NPP. Moreover, our findings suggest that reductions in NPP were largely due to decreases in solar radiation (82%), rather than the commonly expected effects of drought (18%). These findings update our previous knowledge of carbon uptake responses to climate change in terrestrial ecosystems and highlight the potential importance of shortwave radiation in driving vegetation productivity for the region, especially for tropical forests. Further clarification of the effects of precipitation and radiation, particularly the impacts of diffuse radiation, on vegetation photosynthesis should be a future research priority.

Acknowledgments

This work was supported by National Natural Science Foundation of China (31270520), the Key Project in the National Science and Technology Pillar program of China (grant 2013BAC03B00), and U.S. National Science Foundation (NSF) EPSCoR program (NSF-IIA-1301789). S. Running was supported by NASA Earth Observing system MODIS grant (NNX08AG87A). This work used eddy covariance data acquired by the ChinaFLUX and AsiaFLUX, and we thank PIs for sharing the flux tower data. Especially, we appreciate Guirui Yu, Shaoqiang Wang, Honglin He, and Li Zhang of the Institute of Geographic Sciences and Natural Resources Research, Chinese Academy of Sciences, as well as the Associate Editor and two anonymous reviewers for their constructive suggestions and comments on this paper. The data used in this study will be available at http://www.cnern.org.cn/data/initDRsearch?classcode=DPAPER.

References

Anav, A., P. Friedlingstein, M. Kidston, L. Bopp, P. Ciais, P. Cox, C. Jones, M. Jung, R. Myneni, and Z. Zhu (2013), Evaluating the land and ocean components of the global carbon cycling in the CMIP5 Earth System Models, *J. Clim.*, *26*(18), 6801–6843, doi:10.1175/JCLI-D-12-00417.1.

Aubinet, M., A. Grelle, A. Ibrom, Ü. Rannik, J. Moncrieff, T. Foken, A. Kowalski, P. Martin, P. Berbigier, and C. Bernhofer (1999), Estimates of the annual net carbon and water exchange of forests: The EUROFLUX methodology, *Adv. Ecol. Res.*, *30*, 113–175.

Beer, C., et al. (2010), Terrestrial gross carbon dioxide uptake: Global distribution and covariation with climate, *Science*, *329*(5993), 834–838, doi:10.1126/science.1184984.

Betts, A. K., M. Zhao, P. A. Dirmeyer, and A. C. M. Beljaars (2006), Comparison of ERA40 and NCEP/DOE near-surface data sets with other ISLSCP-II data sets, *J. Geophys. Res.*, *111*, D22S04, doi:10.1029/2006JD007174.

Bonan, G. B. (1989), A computer model of the solar radiation, soil moisture, and soil thermal regimes in boreal forests, *Ecol. Modell.*, *45*(4), 275–306.

Cai, W. W., W. P. Yuan, S. L. Liang, X. T. Zhang, W. J. Dong, J. Z. Xia, Y. Fu, Y. Chen, D. Liu, and Q. Zhang (2014), Improved estimations of gross primary production using satellite-derived photosynthetically active radiation, *J. Geophys. Res. Biogeosciences*, *119*, 110–123, doi:10.1002/2013jg002456.

Cao, M., and F. I. Woodward (1998), Dynamic responses of terrestrial ecosystem carbon cycling to global climate change, *Nature*, *393*(6682), 249–252.

Cao, M., B. Tao, K. R. Li, X. M. Shao, and S. D. Prience (2003), Interannual variation in terrestrial ecosystem carbon fluxes in China from 1981 to 1998, *Acta Bot. Sin.*, *45*(5), 552–560.

Chen, B., T. A. Black, N. C. Coops, T. Hilker, J. A. Trofymow, and K. Morgenstern (2009), Assessing tower flux footprint climatology and scaling between remotely sensed and eddy covariance measurements, *Boundary Layer Meteorol.*, *130*(2), 137–167, doi:10.1007/s10546-008-9339-1.

Chen, J., F. Deng, and M. Chen (2006), Locally adjusted cubic-spline capping for reconstructing seasonal trajectories of a satellite-derived surface parameter, *Geosci. Rem. Sens., IEEE Trans.*, *44*(8), 2230–2238, doi:10.1109/TGRS.2006.872089.

Chen, J., M. Shen, and T. Kato (2009), Diurnal and seasonal variations in light-use efficiency in an alpine meadow ecosystem: Causes and implications for remote sensing, *J. Plant Ecol.*, *2*(4), 173–185, doi:10.1093/jpe/rtp020.

Falge, E., D. Baldocchi, R. Olson, P. Anthoni, M. Aubinet, C. Bernhofer, G. Burba, R. Ceulemans, R. Clement, and H. Dolman (2001), Gap filling strategies for defensible annual sums of net ecosystem exchange, *Agr. Forest Meteorol.*, *107*(1), 43–69.

Farr, T. G., P. A. Rosen, E. Caro, R. Crippen, R. Duren, S. Hensley, M. Kobrick, M. Paller, E. Rodriguez, and L. Roth (2007), The shuttle radar topography mission, *Rev. Geophys.*, *45,* RG2004, doi:10.1029/2005RG000183.

Feng, X., G. Liu, J. M. Chen, M. Chen, J. Liu, W. M. Ju, R. Sun, and W. Zhou (2007), Net primary productivity of China's terrestrial ecosystems from a process model driven by remote sensing, *J. Environ. Manage.*, *85*(3), 563–573, doi:10.1016/j.jenvman.2006.09.021.

Foody, G. M. (2002), Status of land cover classification accuracy assessment, *Remote Sens. Environ.*, *80*(1), 185–201.

Friend, A. D., et al. (2007), FLUXNET and modelling the global carbon cycle, *Global Change Biol.*, *13*(3), 610–633, doi:10.1111/j.1365-2486.2006.01223.x.

Fu, C. B., L. Dan, Y. L. Chen, and J. X. Tang (2015), Trends of the sunshine duration and diffuse radiation percentage on sunny days in urban agglomerations of China during 1960–2005, *J. Environ. Sci.-China*, *34*, 206–211, doi:10.1016/j.jes.2014.08.027.

Fu, Y., G.-R. Yu, X.-M. Sun, Y.-N. Li, X.-F. Wen, L.-M. Zhang, Z.-Q. Li, L. Zhao, and Y.-B. Hao (2006), Depression of net ecosystem CO_2 exchange in semi-arid *Leymus chinensis* steppe and alpine shrub, *Agr. Forest Meteorol.*, *137*(3), 234–244.

Gao, Y., G. Yu, L. Zhang, M. Liu, M. Huang, and Q. Wang (2012), The changes of net primary productivity in Chinese terrestrial ecosystem: Based on process and parameter models, *Progr. Geogr.*, *31*(1), 109–117.

Gill, R., R. Kelly, W. Parton, K. Day, R. Jackson, J. Morgan, J. Scurlock, L. Tieszen, J. V. Castle, and D. Ojima (2002), Using simple environmental variables to estimate below-ground productivity in grasslands, *Global Ecol. Biogeogr.*, *11*(1), 79–86.

Gitelson, A. A., A. Vina, S. B. Verma, D. C. Rundquist, T. J. Arkebauer, G. Keydan, B. Leavitt, V. Ciganda, G. G. Burba, and A. E. Suyker (2006), Relationship between gross primary production and chlorophyll content in crops: Implications for the synoptic monitoring of vegetation productivity, *J. Geophys. Res.*, *111*, D08S11, doi:10.1029/2005JD006017.

Guan, D.-X., J.-B. Wu, X.-S. Zhao, S.-J. Han, G.-R. Yu, X.-M. Sun, and C.-J. Jin (2006), CO_2 fluxes over an old, temperate mixed forest in northeastern China, *Agr. Forest Meteorol.*, *137*(3), 138–149.

Guanter, L., et al. (2014), Global and time-resolved monitoring of crop photosynthesis with chlorophyll fluorescence, *Proc. Natl. Acad. Sci. U.S.A.*, *111*(14), E1327–E1333, doi:10.1073/pnas.1320008111.

Haario, H., E. Saksman, and J. Tamminen (2001), An adaptive Metropolis algorithm, *Bernoulli*, *7*, 223–242.

Haario, H., M. Laine, A. Mira, and E. Saksman (2006), DRAM: Efficient adaptive MCMC, *Stat. Comput.*, *16*(4), 339–354.

He, M., et al. (2013), Development of a two-leaf light use efficiency model for improving the calculation of terrestrial gross primary productivity, *Agr. Forest Meteorol.*, *173*, 28–39, doi:10.1016/j.agrformet.2013.01.003.

Hirata, R., N. Saigusa, S. Yamamoto, Y. Ohtani, R. Ide, J. Asanuma, M. Gamo, T. Hirano, H. Kondo, and Y. Kosugi (2008), Spatial distribution of carbon balance in forest ecosystems across East Asia, *Agr. Forest Meteorol.*, *148*(5), 761–775.

Hutchinson, G., and P. McIntosh (2000), Case study of integrated risk assessment mapping in the Southland Region of New Zealand, *Environ. Toxicol. Chem.*, *19*(4 II), 1143–1147.

Ito, A. (2011), A historical meta-analysis of global terrestrial net primary productivity: Are estimates converging?, *Global Change Biol.*, *17*(10), 3161–3175, doi:10.1111/j.1365-2486.2011.02450.x.

Jönsson, P., and L. Eklundh (2004), TIMESAT—A program for analyzing time-series of satellite sensor data, *Comput. Geosci.*, *30*(8), 833–845.

Jung, M., M. Reichstein, and A. Bondeau (2009), Towards global empirical upscaling of FLUXNET eddy covariance observations: Validation of a model tree ensemble approach using a biosphere model, *Biogeosciences*, *6*(10), 2001–2013.

Jung, M., et al. (2011), Global patterns of land-atmosphere fluxes of carbon dioxide, latent heat, and sensible heat derived from eddy covariance, satellite, and meteorological observations, *J. Geophys. Res.*, *116*, G00J07, doi:10.1029/2010JG001566.

Kalnay, E., et al. (1996), The NCEP/NCAR 40-year reanalysis project, *Bull. Am. Meteorol. Soc.*, *77*(3), 437–471, doi:10.1175/1520-0477(1996)077<0437:TNYRP>2.0.CO;2.

Kanamitsu, M., W. Ebisuzaki, J. Woollen, S.-K. Yang, J. Hnilo, M. Fiorino, and G. Potter (2002), NCEP-DOE AMIP-II reanalysis (R-2), *Bull. Am. Meteorol. Soc.*, *83*(11), 1631–1643.

Kanniah, K. D., J. Beringer, L. B. Hutley, N. J. Tapper, and X. Zhu (2009), Evaluation of Collections 4 and 5 of the MODIS gross primary productivity product and algorithm improvement at a tropical savanna site in northern Australia, *Remote Sens. Environ.*, *113*(9), 1808–1822, doi:10.1016/j.rse.2009.04.013.

Keith, H., E. van Gorsel, K. L. Jacobsen, and H. A. Cleugh (2012), Dynamics of carbon exchange in a Eucalyptus forest in response to interacting disturbance factors, *Agr. Forest Meteorol.*, *153*, 67–81, doi:10.1016/j.agrformet.2011.07.019.

Koffi, E. N., P. J. Rayner, M. Scholze, and C. Beer (2012), Atmospheric constraints on gross primary productivity and net ecosystem productivity: Results from a carbon-cycle data assimilation system, *Global Biogeochem. Cycles*, *26*, GB1024, doi:10.1029/2010GB003900.

Krishnaswamy, J., R. John, and S. Joseph (2014), Consistent response of vegetation dynamics to recent climate change in tropical mountain regions, *Global Change Biol.*, *20*(1), 203–215, doi:10.1111/Gcb.12362.

Leuning, R., H. A. Cleugh, S. J. Zegelin, and D. Hughes (2005), Carbon and water fluxes over a temperate Eucalyptus forest and a tropical wet/dry savanna in Australia: Measurements and comparison with MODIS remote sensing estimates, *Agr. Forest Meteorol.*, *129*(3–4), 151–173, doi:10.1016/j.agrformet.2004.12.004.

Li, C., H. He, M. Liu, W. Su, Y. Fu, L. Zhang, X. Wen, and G. Yu (2008), The design and application of CO_2 flux data processing system at ChinaFLUX, *Geo-Infor. Sci.*, *10*(5), 557–565.

Li, D., W. Ju, D. Lu, Y. Zhou, and H. Wang (2015), Impact of estimated solar radiation on gross primary productivity simulation in subtropical plantation in southeast China, *Sol. Ener.*, *120*, 186–175, doi:10.1016/j.solener.2015.07.033.

Li, X., et al. (2013), Estimation of gross primary production over the terrestrial ecosystems in China, *Ecol. Modell.*, *261*, 80–92, doi:10.1016/j.ecolmodel.2013.03.024.

Lin, H. L., J. Zhao, T. G. Liang, J. Bogaert, and Z. Q. Li (2012), A classification indices-based model for net primary productivity (NPP) and potential productivity of vegetation in China, *Int. J. Biomath.*, *5*(3), 145–167, doi:10.1142/S1793524512600091.

Liu, J., M. Liu, D. Zhuang, Z. Zhang, and X. Deng (2003a), Study on spatial pattern of land-use change in China during 1995–2000, *Sci. China Ser. D: Earth Sci.*, *46*(4), 373–384.

Liu, J., Z. Zhang, D. Zhuang, Y. Wang, W. Zhou, S. Zhang, R. Li, N. Jiang, and S. Wu (2003b), A study on the spatial-temporal dynamic changes of land-use and driving forces analyses of China in the 1990s, *Geogr. Res.*, *22*(1), 1–12.

Liu, J., H. Tian, M. Liu, D. Zhuang, J. M. Melillo, and Z. Zhang (2005), China's changing landscape during the 1990s: Large-scale land transformations estimated with satellite data, *Geophys. Res. Lett.*, *32*, L02405, doi:10.1029/2004GL021649.

Liu, J., Z. Zhang, X. Xu, W. Kuang, W. Zhou, S. Zhang, R. Li, C. Yan, D. Yu, and S. Wu (2010), Spatial patterns and driving forces of land use change in China during the early 21st century, *J. Geogr. Sci.*, *20*(4), 483–494.

Liu, J., et al. (2014), Spatiotemporal characteristics, patterns, and causes of land-use changes in China since the late 1980s, *J. Geogr. Sci.*, *24*(2), 195–210, doi:10.1007/s11442-014-1082-6.

Liu, M., H. He, G. Yu, X. Sun, L. Zhang, S. Han, H. Wang, and G. Zhou (2012), Uncertainty analysis in data processing on the estimation of net carbon exchanges at different forest ecosystems in China, *J. Forest Res.*, *17*(3), 312–322.

Liu, Y., W. Ju, H. He, S. Wang, R. Sun, and Y. D. Zhang (2013), Changes of net primary productivity in China during recent 11 years detected using an ecological model driven by MODIS data, *Front. Earth Sci.*, *7*(1), 112–127.

Liu, Z., Q. Shao, and J. Liu (2015), The performances of MODIS-GPP and -ET products in China and their sensitivity to input data (FPAR/LAI), *Rem. Sens.*, *7*(1), 135–152, doi:10.3390/rs70100135.

Luo, T. (1996), *Patterns of Net Primary Productivity for Chinese Major Forest Types and Their Mathematical Models, Commission for the Integrated Survey of Natural Resources*, Chinese Academy of Sciences, Beijing.

Luo, T., W. Li, J. Luo, and Q. Wang (1998), A comparative study on biological production of major vegetation types on the Tibetan Plateau, *Acta Ecol. Sin.*, *19*(6), 823–831.

Luo, T., W. Li, and H. Zhu (2002), Estimated biomass and productivity of natural vegetation on the Tibetan Plateau, *Ecol. Appl.*, *12*(4), 980–997, doi:10.2307/3061031.

Madani, N., J. S. Kimball, D. L. R. Affleck, J. Kattge, J. Graham, P. M. van Bodegom, P. B. Reich, and S. W. Running (2014), Improving ecosystem productivity modeling through spatially explicit estimation of optimal light use efficiency, *J. Geophys. Re. Biogeosciences*, *119*, 1755–1769, doi:10.1002/2014JG002709.

Medlyn, B. E. (2011), Comment on "Drought-Induced Reduction in Global Terrestrial Net Primary Production from 2000 Through 2009", *Science*, *333*(6046), 1093, doi:10.1126/science.1199544.

Melillo, J. M., A. D. McGuire, D. W. Kicklighter, B. Moore, C. J. Vorosmarty, and A. L. Schloss (1993), Global climate change and terrestrial net primary production, *Nature*, *363*(6426), 234–240.

Monteith, J. (1972), Solar radiation and productivity in tropical ecosystems, *J. Appl. Ecol.*, *9*(3), 747–766.

Monteith, J., and C. Moss (1977), Climate and the efficiency of crop production in Britain [and Discussion], *Phil. Trans. Roy. Soc. Lond. Ser. B, Biol. Sci.*, *281*(980), 277–294.

Mu, Q., M. Zhao, F. A. Heinsch, M. Liu, H. Tian, and S. W. Running (2007), Evaluating water stress controls on primary production in biogeochemical and remote sensing based models, *J. Geophys. Res.*, *112,* G01012, doi:10.1029/2006JG000179.

Nightingale, J. M., N. C. Coops, R. H. Waring, and W. W. Hargrove (2007), Comparison of MODIS Gross Primary Production estimates for forests across the USA with those generated by a simple process model, 3-PGS, *Remote Sens. Environ.*, *109*(4), 500–509.

Nightingale, J. M., J. T. Morisette, R. E. Wolfe, B. Tan, F. Gao, G. Ederer, G. J. Collatz, and D. P. Turner (2009), Temporally smoothed and gap-filled MODIS land products for carbon modelling: Application of the fPAR product, *Int. J. Rem. Sens.*, *30*(4), 1083–1090, doi:10.1080/01431160802398064.

Ogutu, B. O., J. Dash, and T. P. Dawson (2013), Developing a diagnostic model for estimating terrestrial vegetation gross primary productivity using the photosynthetic quantum yield and Earth Observation data, *Global Change Biol.*, *19*, 2878–2892, doi:10.1111/gcb.12261.

Pan, Y., R. Birdsey, J. Hom, K. McCullough, and K. Clark (2006), Improved estimates of net primary productivity from MODIS satellite data at regional and local scales, *Ecol. Appl.*, *16*(1), 125–132.

Piao, S., et al. (2014), Evidence for a weakening relationship between interannual temperature variability and northern vegetation activity, *Nat. Commun.*, *5*, 5018, doi:10.1038/ncomms6018.

Piao, S. L., et al. (2015), Detection and attribution of vegetation greening trend in China over the last 30 years, *Global change Biol.*, *21*(4), 1601–1609, doi:10.1111/gcb.12795.

Potter, C. S. (1999), Terrestrial biomass and the effects of deforestation on the global carbon cycle—Results from a model of primary production using satellite observations, *BioScience*, *49*(10), 769–778.

Potter, C. S., J. T. Randerson, C. B. Field, P. A. Matson, P. M. Vitousek, H. A. Mooney, and S. A. Klooster (1993), Terrestrial ecosystem production—A process model-based on global satellite and surface data, *Global Biogeochem. Cycles*, *7*, 811–841, doi:10.1029/93GB02725.

Prince, S. D., and S. J. Goward (1995), Global primary production: A remote sensing approach, *J. Biogeogr.*, *22*, 316–336.

Quaife, T., S. Quegan, M. Disney, P. Lewis, M. Lomas, and F. I. Woodward (2008), Impact of land cover uncertainties on estimates of biospheric carbon fluxes, *Global Biogeochem. Cycles*, *22*, GB4016, doi:10.1029/2007GB003097.

Rabus, B., M. Eineder, A. Roth, and R. Bamler (2003), The shuttle radar topography mission—A new class of digital elevation models acquired by spaceborne radar, *ISPRS J. Photogramm. Remote Sens.*, *57*(4), 241–262.
Raczka, B. M., et al. (2013), Evaluation of continental carbon cycle simulations with North American flux tower observations, *Ecol. Monogr.*, *83*(4), 531–556, doi:10.1890/12-0893.1.
Reichstein, M., et al. (2005), On the separation of net ecosystem exchange into assimilation and ecosystem respiration: Review and improved algorithm, *Global Change Biol.*, *11*(9), 1424–1439, doi:10.1111/j.1365-2486.2005.001002.x.
Ren, X. L., H. L. He, L. Zhang, and G. R. Yu (2014), Estimation of diffuse photosynthetically active radiation and the spatiotemporal variation analysis in China from 1981 to 2010, *J. Geogr. Sci.*, *24*(4), 579–592, doi:10.1007/s11442-014-1107-1.
Running, S. W. (2013), Approaching the limits, *Science*, *339*(6125), 1276–1277, doi:10.1126/science.1235886.
Running, S. W., P. E. Thornton, R. Nemani, and J. M. Glassy (2000), Global terrestrial gross and net primary productivity from the Earth Observing System, in *Methods in Ecosystem Science*, edited by O. E. Sala et al., pp. 44–57, Springer Verlag, New York.
Running, S. W., R. R. Nemani, F. A. Heinsch, M. Zhao, M. Reeves, and H. Hashimoto (2004), A continuous satellite-derived measure of global terrestrial primary production, *BioScience*, *54*(6), 547–560.
Samanta, A., M. H. Costa, E. L. Nunes, S. A. Vieira, L. Xu, and R. B. Myneni (2011), Comment on "Drought-Induced Reduction in Global Terrestrial Net Primary Production from 2000 Through 2009", *Science*, *333*(6046), 1093, doi:10.1126/science.1199048.
Schaefer, K., C. R. Schwalm, C. Williams, M. A. Arain, A. Barr, J. M. Chen, K. J. Davis, D. Dimitrov, T. W. Hilton, and D. Y. Hollinger (2012), A model-data comparison of gross primary productivity: Results from the North American Carbon Program site synthesis, *J. Geophys. Res.*, *117*, G03010, doi:10.1029/2012JG001960.
Schimel, D. S., V. Participants, and B. H. Braswell (1997), Continental scale variability in ecosystem processes: Models, data, and the role of disturbance, *Ecol. Monogr.*, *67*(2), 251–271.
Schwalm, C. R., et al. (2010), A model-data intercomparison of CO_2 exchange across North America: Results from the North American Carbon Program site synthesis, *J. Geophys. Res.*, *115*, G00H05, doi:10.1029/2009JG001229.
Sims, D. A., et al. (2006), On the use of MODIS EVI to assess gross primary productivity of North American ecosystems, *J. Geophys. Res.*, *111*, G04015, doi:10.1029/2006JG000162.
Sims, D. A., et al. (2008), A new model of gross primary productivity for North American ecosystems based solely on the enhanced vegetation index and land surface temperature from MODIS, *Remote Sens. Environ.*, *112*(4), 1633–1646, doi:10.1016/j.rse.2007.08.004.
Sjostrom, M., et al. (2011), Exploring the potential of MODIS EVI for modeling gross primary production across African ecosystems, *Remote Sens. Environ.*, *115*(4), 1081–1089, doi:10.1016/j.rse.2010.12.013.
Sjostrom, M., et al. (2013), Evaluation of MODIS gross primary productivity for Africa using eddy covariance data, *Remote Sens. Environ.*, *131*, 275–286, doi:10.1016/j.rse.2012.12.023.
Smith, W. K., S. C. Reed, C. C. Cleveland, A. P. Ballantyne, W. R. L. Anderegg, W. R. Wieder, Y. Y. Liu, and S. W. Running (2016), Large divergence of satellite and Earth system model estimates of global terrestrial CO_2 fertilization, *Nat. Clim. Change*, *6*(3), 306–310, doi:10.1038/nclimate2879.
Tian, H., et al. (2011), China's terrestrial carbon balance: Contributions from multiple global change factors, *Global Biogeochem. Cycles*, *25*, GB1007, doi:10.1029/2010GB003838.
Turner, D. P., et al. (2006), Evaluation of MODIS NPP and GPP products across multiple biomes, *Remote Sens. Environ.*, *102*(3-4), 282–292, doi:10.1016/j.rse.2006.02.017.
Wagle, P., X. Xiao, M. S. Torn, D. R. Cook, R. Matamala, M. L. Fischer, C. Jin, J. Dong, and C. Biradar (2014), Sensitivity of vegetation indices and gross primary production of tallgrass prairie to severe drought, *Remote Sens. Environ.*, *152*, 1–14, doi:10.1016/j.rse.2014.05.010.
Wang, J., J. Liu, M. Cao, Y. Liu, G. Yu, G. Li, S. Qi, and K. Li (2011), Modelling carbon fluxes of different forests by coupling a remote-sensing model with an ecosystem process model, *Int. J. Rem. Sens.*, *32*(21), 6539–6567, doi:10.1080/01431161.2010.512933.
Wang, J., et al. (2014), Comparison of gross primary productivity derived from GIMMS NDVI3g, GIMMS, and MODIS in Southeast Asia, *Rem. Sens.*, *6*(3), 2108–2133.
Wang, S. Q., et al. (2015), Improving the light use efficiency model for simulating terrestrial vegetation gross primary production by the inclusion of diffuse radiation across ecosystems in China, *Ecol. Complex.*, *23*, 1–13, doi:10.1016/j.ecocom.2015.04.004.
Webb, E. K., G. I. Pearman, and R. Leuning (1980), Correction of flux measurements for density effects due to heat and water vapour transfer, *Q. J. R. Meteorol. Soc.*, *106*(447), 85–100, doi:10.1002/qj.49710644707.
Welp, L. R., R. F. Keeling, H. A. Meijer, A. F. Bollenbacher, S. C. Piper, K. Yoshimura, R. J. Francey, C. E. Allison, and M. Wahlen (2011), Interannual variability in the oxygen isotopes of atmospheric CO_2 driven by El Niño, *Nature*, *477*(7366), 579–582.
Wen, X.-F., G.-R. Yu, X.-M. Sun, Q.-K. Li, Y.-F. Liu, L.-M. Zhang, C.-Y. Ren, Y.-L. Fu, and Z.-Q. Li (2006), Soil moisture effect on the temperature dependence of ecosystem respiration in a subtropical *Pinus* plantation of southeastern China, *Agr. Forest Meteorol.*, *137*(3), 166–175.
Wu, C., Z. Niu, and S. A. Gao (2010a), Gross primary production estimation from MODIS data with vegetation index and photosynthetically active radiation in maize, *J. Geophys. Res.*, *115*, D12127, doi:10.1029/2009JD013023.
Wu, C., J. W. Munger, Z. Niu, and D. Kuang (2010b), Comparison of multiple models for estimating gross primary production using MODIS and eddy covariance data in Harvard Forest, *Remote Sens. Environ.*, *114*(12), 2925–2939, doi:10.1016/j.rse.2010.07.012.
Wu, C., J. M. Chen, and N. Huang (2011), Predicting gross primary production from the enhanced vegetation index and photosynthetically active radiation: Evaluation and calibration, *Remote Sens. Environ.*, *115*(12), 3424–3435, doi:10.1016/j.rse.2011.08.006.
Wu, C., A. Gonsamo, F. M. Zhang, and J. M. Chen (2014), The potential of the greenness and radiation (GR) model to interpret 8-day gross primary production of vegetation, *ISPRS J. Photogramm. Remote Sens.*, *88*, 69–79.
Wu, Z., P. Dijkstra, G. W. Koch, J. Penuelas, and B. A. Hungate (2011), Responses of terrestrial ecosystems to temperature and precipitation change: A meta-analysis of experimental manipulation, *Global Change Biol.*, *17*(2), 927–942, doi:10.1111/j.1365-2486.2010.02302.x.
Xiao, J., Y. Zhou, and L. Zhang (2015), Contributions of natural and human factors to increases in vegetation productivity in China, *Ecosphere*, *6*(11), doi:10.1890/es14-00394.1.
Xiao, X. M., Q. Y. Zhang, B. Braswell, S. Urbanski, S. Boles, S. Wofsy, M. Berrien, and D. Ojima (2004), Modeling gross primary production of temperate deciduous broadleaf forest using satellite images and climate data, *Remote Sens. Environ.*, *91*(2), 256–270, doi:10.1016/j.rse.2004.03.010.
Xin, Q., M. Broich, A. E. Suyker, L. Yu, and P. Gong (2015), Multi-scale evaluation of light use efficiency in MODIS gross primary productivity for croplands in the Midwestern United States, *Agr. Forest Meteorol.*, *201*, 111–119, doi:10.1016/j.agrformet.2014.11.004.
Yan, H., et al. (2015), Improved global simulations of gross primary product based on a new definition of water stress factor and a separate treatment of C3 and C4 plants, *Ecol. Modell.*, *297*, 42–59, doi:10.1016/j.ecolmodel.2014.11.002.
Yang, K., T. Koike, and B. Ye (2006), Improving estimation of hourly, daily, and monthly solar radiation by importing global data sets, *Agr. Forest Meteorol.*, *137*(1–2), 43–55, doi:10.1016/j.agrformet.2006.02.001.

Yang, Y., S. Shang, H. Guan, and L. Jiang (2013), A novel algorithm to assess gross primary production for terrestrial ecosystems from MODIS imagery, *J. Geophys. Res. Biogeosciences*, *118*, 590–605, doi:10.1002/jgrg.20056.

Yi, Y., J. S. Kimball, L. A. Jones, R. H. Reichle, and K. C. McDonald (2011), Evaluation of MERRA land surface estimates in preparation for the soil moisture active passive mission, *J. Clim.*, *24*(15), 3797–3816, doi:10.1175/2011JCLI4034.1.

Yi, Y., J. S. Kimball, L. A. Jones, R. H. Reichle, R. Nemani, and H. A. Margolis (2013), Recent climate and fire disturbance impacts on boreal and arctic ecosystem productivity estimated using a satellite-based terrestrial carbon flux model, *J. Geophys. Res. Biogeosciences*, *118*, 606–622, doi:10.1002/jgrg.20053.

Yu, G., X. Wen, X. Sun, B. D. Tanner, X. Lee, and J. Chen (2006), Overview of ChinaFLUX and evaluation of its eddy covariance measurement, *Agr. Forest Meteorol.*, *137*(3–4), 125–137, doi:10.1016/j.agrformet.2006.02.011.

Yu, G., et al. (2013), Spatial patterns and climate drivers of carbon fluxes in terrestrial ecosystems of China, *Global Change Biol.*, *19*(3), 798–810, doi:10.1111/gcb.12079.

Yu, G., Z. Chen, S. Piao, C. Peng, P. Ciais, Q. Wang, X. Li, and X. Zhu (2014), High carbon dioxide uptake by subtropical forest ecosystems in the East Asian monsoon region, *Proc. Natl. Acad. Sci. U.S.A.*, *111*(13), 4910–4915.

Yuan, Q., S. Wu, D. Zhao, E. Dai, L. Chen, and L. Zhang (2014), Modeling net primary productivity of the terrestrial ecosystem in China from 1961 to 2005, *J. Geogr. Sci.*, *24*(1), 3–17, doi:10.1007/s11442-014-1069-3.

Yuan, W., et al. (2010), Global estimates of evapotranspiration and gross primary production based on MODIS and global meteorology data, *Remote Sens. Environ.*, *114*(7), 1416–1431.

Yuan, W., et al. (2014a), Multiyear precipitation reduction strongly decreases carbon uptake over northern China, *J. Geophys. Res. Biogeosciences*, *119*, 881–896, doi:10.1002/2014jg002608.

Yuan, W., et al. (2014b), Global comparison of light use efficiency models for simulating terrestrial vegetation gross primary production based on the LaThuile database, *Agr. Forest Meteorol.*, *192–193*, 108–120, doi:10.1016/j.agrformet.2014.03.007.

Yuan, W., et al. (2016), Severe summer heatwave and drought strongly reduced carbon uptake in Southern China, *Sci. Rep.*, *6*(18813), 18,813, doi:10.1038/srep18813.

Zhang, H., R. Shi, H. Zhong, P. Qu, J. Sun, W. Lin, and S. Li (2009), Improvement of MODIS 8-day LAI/FPAR product with temporal filters to generate high quality time-series product, in *2009 Joint Urban Remote Sensing Event*, edited, pp. 162–168, IEEE, Shanghai, China.

Zhang, L.-M., G.-R. Yu, X.-M. Sun, X.-F. Wen, C.-Y. Ren, Y.-L. Fu, Q.-K. Li, Z.-Q. Li, Y.-F. Liu, and D.-X. Guan (2006), Seasonal variations of ecosystem apparent quantum yield (α) and maximum photosynthesis rate (P_{max}) of different forest ecosystems in China, *Agr. Forest Meteorol.*, *137*(3), 176–187.

Zhang, P., S. P. Chen, W. L. Zhang, H. X. Miao, J. Q. Chen, X. G. Han, and G. H. Lin (2012), Biophysical regulations of NEE light response in a steppe and a cropland in Inner Mongolia, *J. Plant Ecol.*, *5*(2), 238–248, doi:10.1093/jpe/rtr017.

Zhang, Y. L., C. H. Song, K. R. Zhang, X. L. Cheng, L. E. Band, and Q. F. Zhang (2014), Effects of land use/land cover and climate changes on terrestrial net primary productivity in the Yangtze River Basin, China, from 2001 to 2010, *J. Geophys. Res. Biogeosciences*, *119*, 1092–1109, doi:10.1002/2014jg002616.

Zhang, Y. Q., Q. Yu, J. Jiang, and Y. H. Tang (2008), Calibration of Terra/MODIS gross primary production over an irrigated cropland on the North China Plain and an alpine meadow on the Tibetan Plateau, *Global Change Biol.*, *14*(4), 757–767, doi:10.1111/j.1365-2486.2008.01538.x.

Zhao, M., and S. W. Running (2010), Drought-induced reduction in global terrestrial net primary production from 2000 through 2009, *Science*, *329*(5994), 940–943, doi:10.1126/science.1192666.

Zhao, M., C. Fu, X. Yan, and G. Wen (2001), Study on the relationship between different ecosystems and climate in China using NOAA/AVHRR data, *Acta Geogr. Sin.*, *56*(3), 287–296.

Zhao, M., F. A. Heinsch, R. R. Nemani, and S. W. Running (2005), Improvements of the MODIS terrestrial gross and net primary production global data set, *Remote Sens. Environ.*, *95*(2), 164–176, doi:10.1016/j.rse.2004.12.011.

Zhao, M., S. W. Running, and R. R. Nemani (2006), Sensitivity of Moderate Resolution Imaging Spectroradiometer (MODIS) terrestrial primary production to the accuracy of meteorological reanalyses, *J. Geophys. Res.*, *111*, G01002, doi:10.1029/2004JG000004.